Microstructural Evolution in ZK60 Magnesium Alloy during Severe Plastic Deformation

Arthur Galiyev and Rustam Kaibyshev

Institute for Metals Superplasticity Problems, Ufa 450001, Russia

A ZK60 alloy was subjected to severe plastic deformation by torsion straining under high pressure at ambient temperature. The data of microhardness measurements, X-ray analysis and TEM observation showed that intense plastic straining resulted in formation of nanometer-scale structure characterized by presence of high internal stress fields. The effect of phase composition of the magnesium alloy on the formation of ultrafine grain structure was examined. It was shown that prior aging promoted the formation of fully grained structure during severe plastic deformation. At the same time, the size of new grains formed was found to be smaller in the quenched state of the magnesium alloy than in the aged state. Grain formation during intense plastic straining was interpreted in terms of low temperature dynamic recrystallization. The mechanisms of ultrafine grain structure formation in hcp material during severe plastic deformation and the role of non-basal slip in this process are discussed.

Keywords: *magnesium alloy, microstructural evolution, intense plastic straining, low temperature dynamic recrystallization, nanometer-scale grains*

1. Introduction

Investigations of microstructural evolution during severe plastic deformation at ambient temperature are of great deal of interest due to the growing importance of producing materials with grain size lying in the submicrometer and nanometer range. The most of the works were dedicated to the examination of microstructure refinement during severe plastic deformation in materials with bcc and fcc lattice.[1–3] Only a limited number of studies dealt with examination of microstructural evolution of hcp materials during intense plastic straining (IPS)[4–6] in spite of the fact that mechanical properties of these materials are very sensitive to grain size and grain refinement can provide a significant increase in yield stress. Some important aspects of ultrafine grain formation in such materials are still unknown. It is obvious that behavior of materials with hcp lattice during IPS has specific features which are very important for developing thermomechanical treatment suitable for producing submicrometer and nanoscale structure in these materials.

It was reported by Mabuchi *et al.*[7] that equal channel angular extrusion (ECAE) is an effective route for refining microstructure of a Mg-based alloy down to micrometer and submicrometer levels. The authors demonstrated that intense plastic straining at $t = 175°C$ produced ultrafine grain structure in the AZ91 magnesium alloy with an average grain size of about 0.5 μm. Following temperature decrease results in sample damage during ECAE processing of a magnesium alloy. Torsion loading under high pressure is the method preferred to subject magnesium alloys by IPS at room temperature.[5,6] The aim of present study is to report the microstructural evolution during severe plastic deformation of a ZK60 magnesium alloy resulting in formation of nanometer-scale grains. Specific attention is paid to examination of influence of phase composition of a material on the resulting structure.

2. Experimental Procedure

Two states of the cast magnesium alloy Mg–5.8%Zn–0.65%Zr (in mass%) with an initial grain size of 85 μm were used in the present work. Samples of first state were quenched from $t = 450°C$. Samples of second state were quenched from the same temperature and then aged at $t = 175°C$ for 4 h. In the state 1 the particles of a secondary phase had a equiaxed shape and their volume fraction did not exceed 5%. In the state 2 the dispersion particles had a lamellar shape and their volume fraction was about 15%.

The disc shaped samples of 10 mm diameter and 0.3 mm thickness were deformed by torsion under high pressure[8] at ambient temperature. True strain, e, was estimated by use of the expression

$$e = \ln(\phi \times r/d), \tag{1}$$

where ϕ is an angular displacement, r is the radius of the tested sample and d is the thickness. Strain rate was about $10^{-2}\,s^{-1}$. The values of the strain rate sensitivity ($m = \partial(\lg \sigma)/\partial(\lg \dot{\varepsilon})$) were determined by strain-rate-jump tension tests by using small scale samples cut from the discs strained. The microstructures of deformed samples were examined at the distance of 3 mm away from the center of sample by using an Olympus PME-3 optical microscope, a JSM-840 scanning electron microscope (SEM) and a JEM-2000EX transmission electron microscope (TEM). X-ray analysis was also performed to define the texture and X-ray physical line broadening. The coherent domain size and internal elastic strain were determined using the Williamson-Hall method.

3. Results

3.1 Mechanical behavior

The microhardness of the as-processed samples is shown in Fig. 1 as a function of true strain. The curves differ strongly from that for the pure magnesium.[5] Plastic deformation yields strong increase in the microhardness of ZK60 alloy. No significant difference in the values of microhardness was found between recrystallized and non-recrystallized areas. At the same time the microhardness behavior is dependent on the initial state of the magnesium alloy.

Strain up to $e = 0.5$ results in a microhardness increase by

about 60% in the both states of the ZK60 alloy. The strain hardening is slightly greater in the state 1.

At $e = 1$, the microhardness in the state 1 is greater than that in the state 2 by a factor of about 1.3. Two stages of strain hardening are observed in the state 1. At strain less than 1, the stage of extensive hardening takes place and results in microhardness increment in two times. In the strain range 1–7, the stage of a gradual microhardness increment is observed. At the second stage, the rise in microhardness is about 20%.

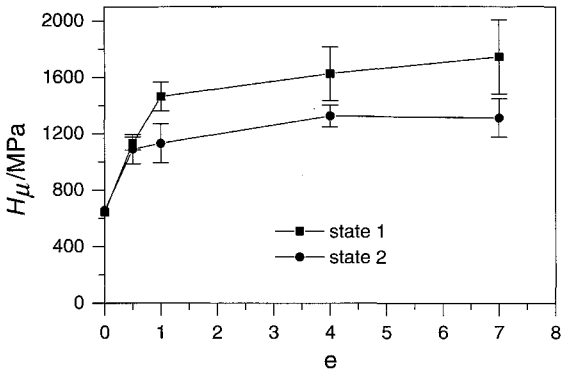

Fig. 1 Microhardness as a function of true strain.

Three stages of plastic deformation may be distinguished in the state 2. At strain less than 0.5, the stage of extensive strain hardening takes place, and microhardness increases by a factor of about 1.5. In the true strain range 0.5–1, the strain hardening rate decreases significantly, and the steady stage is attained after a true strain of 4.

The coefficient of strain rate sensitivity increases insignificantly from $m = 0.08$ in the initial state up to $m = 0.12$ with increasing strain up to $e = 4$ in the both states of the magnesium alloy.

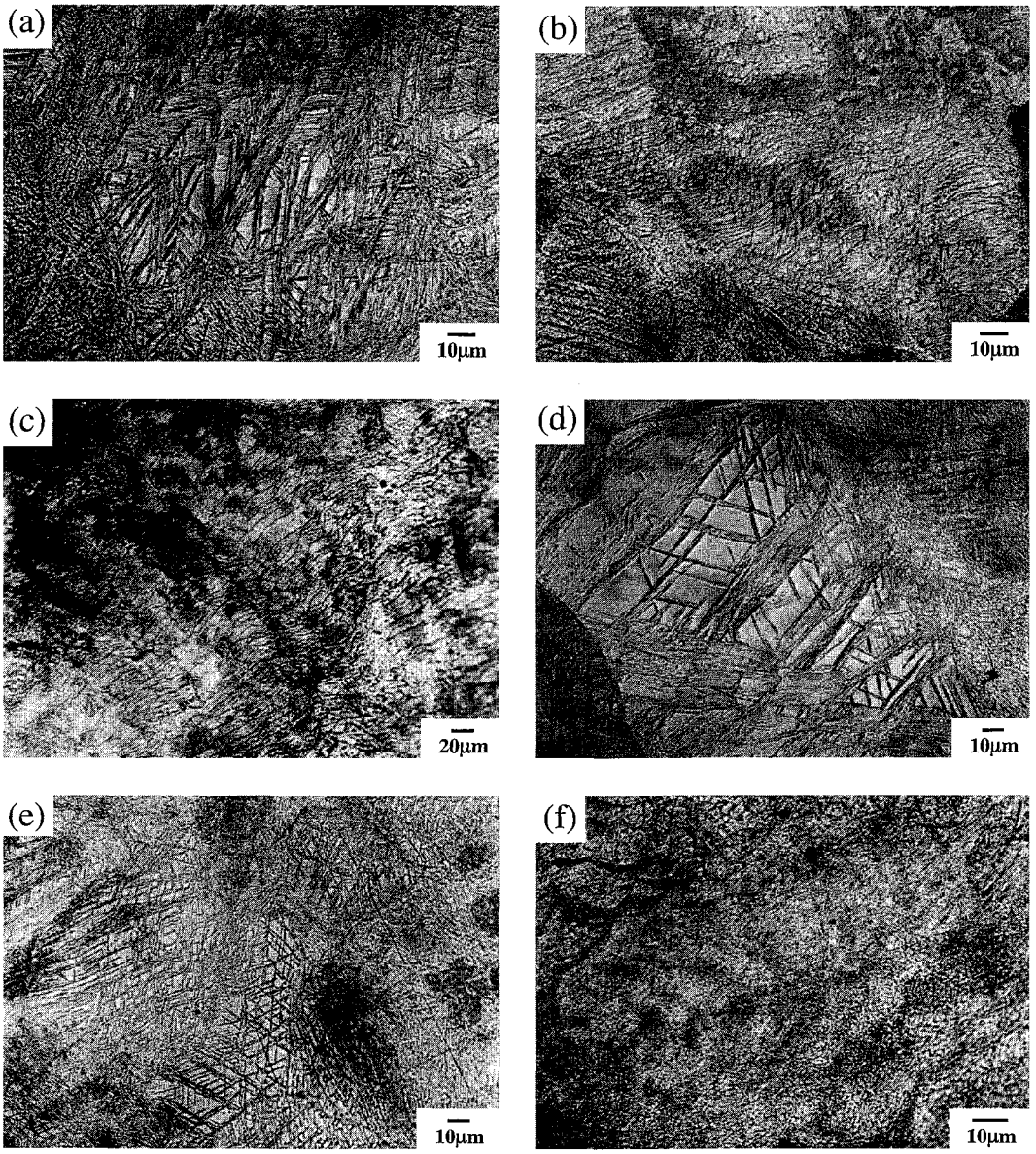

Fig. 2 Effect of strain on microstructures. (a) state 1, $e = 0.5$; (b) state 1, $e = 1$; (c) state 1, $e = 4$; (d) state 2, $e = 0.5$; (e) state 2, $e = 1$; (f) state 2, $e = 4$.

Table 1 Twin volume fraction (%) as a function of true strain.

	$e = 0.5$	$e = 1$
State 1	28.5	46.7
State 2	17.6	29.8

3.2 Microstructure

Plastic deformation of ZK60 alloy results in twinning and the formation of new grains in the both states of the material (Fig. 2, Table 1). On the other hand the microstructural evolution differs significantly in two states.

An evidence for extensive twinning was found in the state 1 after a true strain of 0.5 (Fig. 2(a)). The coarse twins pass entirely across several grains. The number of non-parallel twin systems is no more than 3. In other grains the conglomerations of thin small twins were observed. In the state 2 the volume fraction of twinned areas is essentially less (Fig. 2(d), Table 1). Areas of ultrafine recrystallized grains were revealed. Notably the size of new grains formed is too small to be revealed by optical metallography technique. However, the areas of new grains can be recognized by a specific etching contrast.

At $e = 1$, the density of twinned areas increases in the both states of the magnesium alloy (Figs. 2(b) and (e), Table 1). The secondary twinning occurs into coarse twinned areas and the formation of new grains was observed here. In the state 2 the structural changes are characterized by the formation of recrystallized grain areas inside the twinning orientations (Fig. 2(e)).

Further plastic deformation up to $e = 4$ results in an increase in volume fraction of recrystallized grain areas (Figs. 2(c), (f) and 3). In the state 2 almost all the material volume consists of recrystallized grains. Therefore, the rate of new grain formation during IPS in the state 2 is essentially higher than that in the state 1. The first new fine grains are formed after a true strain of 0.5 in the state 2 and after $e = 4$ the recrystallization is almost completed. In the state 1 the new grains appear only after $e = 1$ and recrystallization does not complete even after the largest true strain of 7.

3.3 Deformation relief

Surface observations (Fig. 4) revealed only basal slip features inside the unrecrystallized areas of initial grains in the state 1. The long straight slip lines pass entirely across grains (Fig. 4(a)). In the same time the wavy slip lines were observed in several grains (Fig. 4(b)). Other slip systems were not revealed. The slip lines in fine grains were not found. No surface dislocation features were revealed in the state 2 either. It is indicative for high uniformity of dislocation glide.

3.4 X-ray diffraction analysis

3.4.1 Texture analysis

The inverse pole figures for two states of ZK60 alloy are shown in Fig. 5. It can be seen that texture changes depend on previous heat treatment of alloy. In the both states the plastic deformation leads to the formation of basal texture and its following spreading at large strain. However these changes occur differently in the two states of the magnesium alloy.

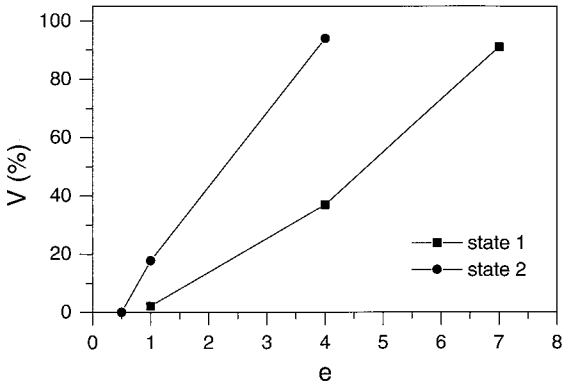

Fig. 3 Volume fraction of recrystallized grains as a function of true strain.

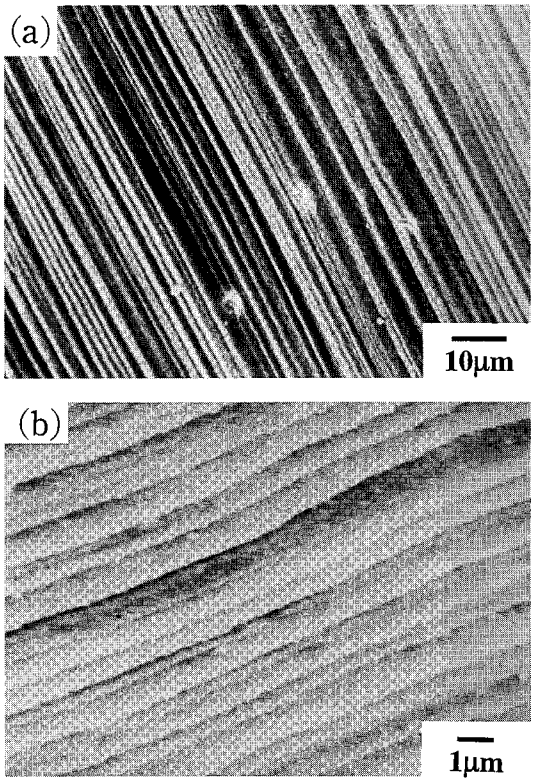

Fig. 4 Deformation relief for state 1.

In the state 1 the weights of the (0001) and $\{10\bar{1}4\}$ orientations increase sharply after $e = 0.5$. The other orientations are weak. The texture close to basal is formed after $e = 0.5$ and changes insignificantly in the strain range 0.5–4. The weight of the (0001) orientation after a true strain of 4 is only about 30% larger than that $e = 0.5$. Notably the weights of the first and second kinds of pyramidal planes slightly increase with strain. Further plastic deformation up to $e = 7$ results in spreading the (0001) orientation and an increment of pyramidal and prismatic orientations.

In the state 2 the texture maximum is about 20% smaller than that in the state 1 after a true strain of 0.5. The larger weights have intermediate $\{20\bar{2}1\}$, $\{10\bar{1}1\}$, $\{10\bar{1}2\}$, $\{11\bar{2}2\}$ orientations. No significant changes occur in the strain range 0.5–1. With further straining to $e = 4$ the weights of pyramidal and prismatic orientations increase and the weight of

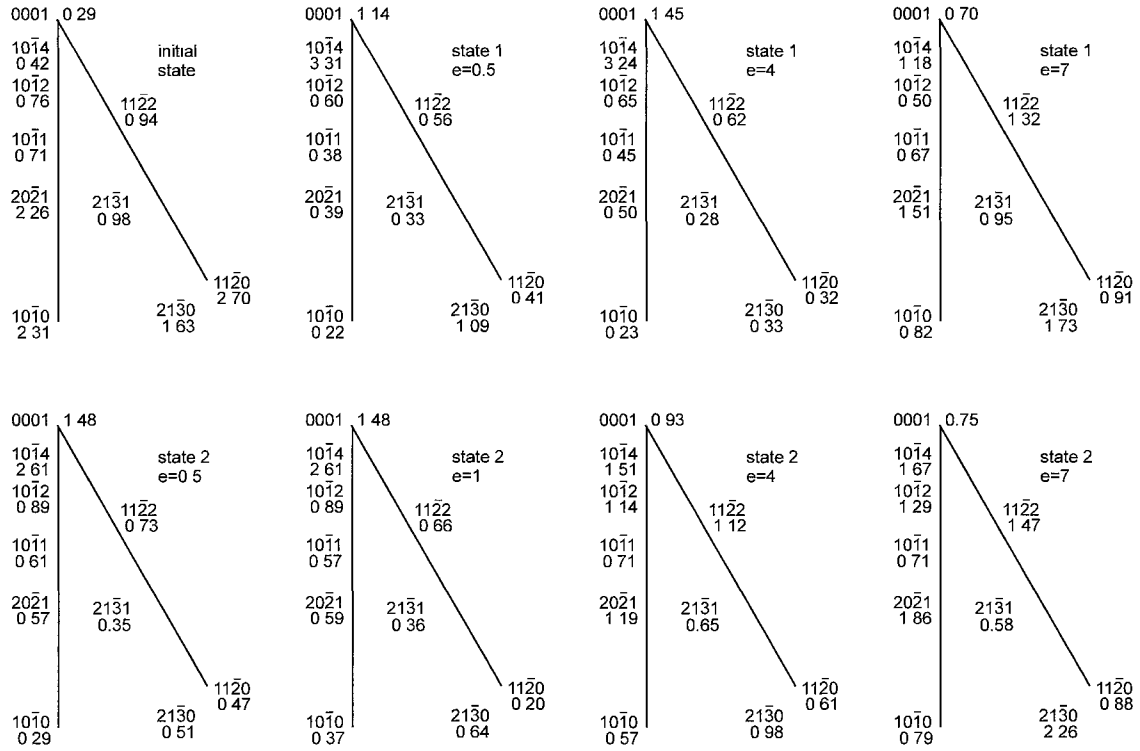

Fig. 5 Inverse pole figures.

(0001) orientation tends to reduce.

3.4.2 X-ray physical line broadening

The results of the X-ray physical line broadening analysis are presented in Fig. 6 for strains $e \geq 0.5$. In all the range of strains the value of the X-ray physical line broadening β is smaller in the state 2 (Fig. 6(a)). At initial stage of plastic deformation the β value increases sharply in the both states. With further straining the values β for lines (0002) and (0004) are changed in different ways. These differences are caused by changes in contributions of the internal elastic strain, n, and coherent domain size, m, into the physical line broadening for the two states of the magnesium alloy (Fig. 6(b)).

In the state 1 the internal elastic strain is predominant at $e = 0.5$ (Fig. 6(b)). Strain increase up to $e = 1$ leads to reduction in the internal elastic strain and a sharp decrease in the coherent domain size (Figs. 6(c) and (d)). In the true strain range 1–7 the contribution of the coherent domain size is major (Fig. 6(b)).

In the state 2 the value of internal elastic strain is about 10% less than that in the state 1 after $e = 0.5$ (Fig. 6(c)). At $e = 1$, the contribution from the coherent domain size is about 30% larger than the one from the internal elastic strain (Fig. 6(b)). Further plastic deformation leads to gradual increase in the relationship m/n in the state 2 and, as a result, the contribution from the coherent domain size becomes major in the state 1 at a true strain of 4 (Fig. 6(b)). It is necessary to notice that the values of internal elastic strain are always less in the state 2 comparing to the state 1.

3.5 Transmission electron microscopy

In the state 1 the areas of high density of tangled lattice dislocations are observed at $e = 0.5$ (Fig. 7(a)). Dislocations with the Burgers vector, $\boldsymbol{a}$, lying into basal planes compose dislocation pile-ups. Areas of dislocation pile-ups of about 0.1–0.3 μm in width and 1 μm in length can be observed. The diffraction spots from the areas of dislocation pile-ups on selected area electron diffraction (SAED) patterns are strongly diffused. It is indicative for high continuous misorientation. Total misorientation of an initial grain may reach several tens degrees. These misorientations are not homogeneous inside the initial grains. It is possible to observe areas with width of 100–300 nm where dislocation pile-ups exhibit uniform contrast as well as areas with width of 150–600 nm where dislocation pile-ups are not exhibited. The azimuthal spreading of diffraction spots from areas of dislocation pile-ups may reach an angle of 30°. It was found that several weak spots are subdivided into several separate spots. It is indicative for evolving new crystallites surrounded by high-angled boundaries.

In the state 2 there exist two structural components after $e = 0.5$. The first component consisting of dislocation pile-ups dominates (Fig. 7(b)). In addition, the second structural component consisting of crystallites with a size of 80–100 nm is observed (Fig. 7(c)). The SAED patterns exhibit diffracted beams scattered around rings, thus indicating the presence of a granular structure separated by high-angled boundaries (Fig. 7(c)). It can be seen that the diffraction patterns from these structural components contain many spots which belong to one zone axis but are misorientated on definite angles between themselves. Some of them are stretched in azimuthal direction. Others have a round shape. Moire patterns are often observed inside the crystallites. The areas of crystallites alternate with the areas of dislocation pile-ups with a size of 100–200 nm. Analysis of diffraction patterns allows to define these areas as a mixture of crystallites and dislocation

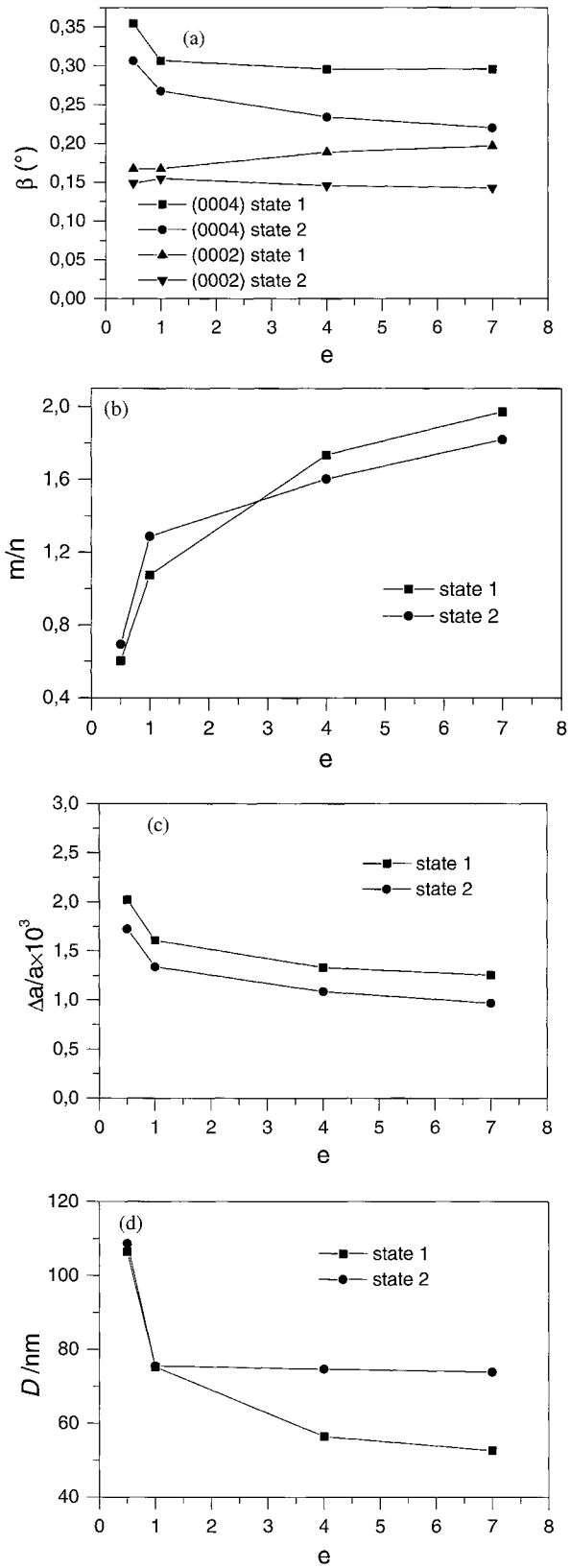

Fig. 6 Evolution of X-ray physical line broadening (a), relationship between contributions of the internal elastic strain, n, and coherent domain size, m, into X-ray physical line broadening (b), internal elastic strain (c) and coherent domain size (d) as a function of true strain.

pile-ups. It is important to notice that continuous misorientation in these areas transforms into discrete misorientation with increasing strain. The close values of azimuthal angles of mutual misorientation between homogeneous areas of the dislocation pile-ups and grains is an evidence for it (Table 2).

With following straining up to $e = 1$ the misorientation of dislocation pile-ups increases in the state 1 (Table 2). It can be evident from a decrease in the size of dislocation pile-ups exhibiting uniform image contrast to 150–200 nm and an increase in diffusivity of diffraction spots toward azimuthal direction (Fig. 8(a)). The new crystallites can be revealed in areas of dislocation pile-ups of high density (Fig. 8(b)). The new grains and misorientated dislocation pile-ups exhibit rectangular shape in contrast to the state 2.

In the state 2 the first structural component transforms into the second one after $e = 1$. The mixture structure consisting of the grains with an average size of 90 nm and dislocation pile-ups was observed (Fig. 8(c)). The SAED patterns show that the number of grains evolved and azimuthal spot scattering (10–16°) are higher in comparison with the state 1. The image contrast from such structural component indicates an existence of the large fields of non-compensated elastic stresses. The large (about 1 μm) dislocation pile-ups were rarely observed. Their continuous misorientation is less than that in the state 1 (Table 2).

Plastic deformation up to $e = 4$ leads to an increase of crystallite volume fraction. Formation of crystallites is almost finished in the state 2 (Fig. 9(b)). In the state 1 the mixture structure consisting of grains and dislocation pile-ups was observed. It is similar with second structural component described above for the state 2 at $e = 1$. A feature of this structure is an elongation of new grains (Fig. 9(a)). The diffraction patterns from this structural component consist of rings of sharp spots. Stretching into azimuthal direction does not exceeded several degrees. The grains have a size of 200–250 nm in length and 50–100 nm in width. They are fully revealed in a reflected position when the dislocation pile-ups are contained in them. If dislocations are not encountered inside the grains or a grain contains few dislocations, the image contrast in these grains is highly distorted by very high elastic stress fields. The reflexes from such areas on diffraction patterns have a considerable azimuthal spreading of about 10°. The areas of dislocation pile-ups are apparently too similar to those described at less strains.

In the state 2 the structure becomes considerably more homogeneous after $e = 4$. The areas with contrast distorted by elastic stresses were almost not observed. The azimuthal spreading of diffraction spots on angles more than 4–6° takes place very rarely and, as a rule, in the areas of non-recrystallized structure. Three types of crystallites can be distinguished. The fine grains ($\leq$ 100 nm) are typically not distorted by elastic stresses (Figs. 9(b) and (c)). Their boundaries exhibit extinction contrast in kind of one dark line. The large elastic stresses and separate dislocations take place in the new grains of second type with a size of about 140 nm (Figs. 9(b) and (c)). The extinction contrast of their boundaries usually exhibits specific alternation of one dark line and one white line.[9] This type of diffraction contrast is usually interpreted as a result of high density of grain boundary dislocations.[7,9] Sometimes Moire patterns appear at these areas. The new grains of third type with a size of 200 nm and above contain dislocation pile-ups (Fig. 9(b)). The extinction contours are either not exhibited or similar to that for grains of

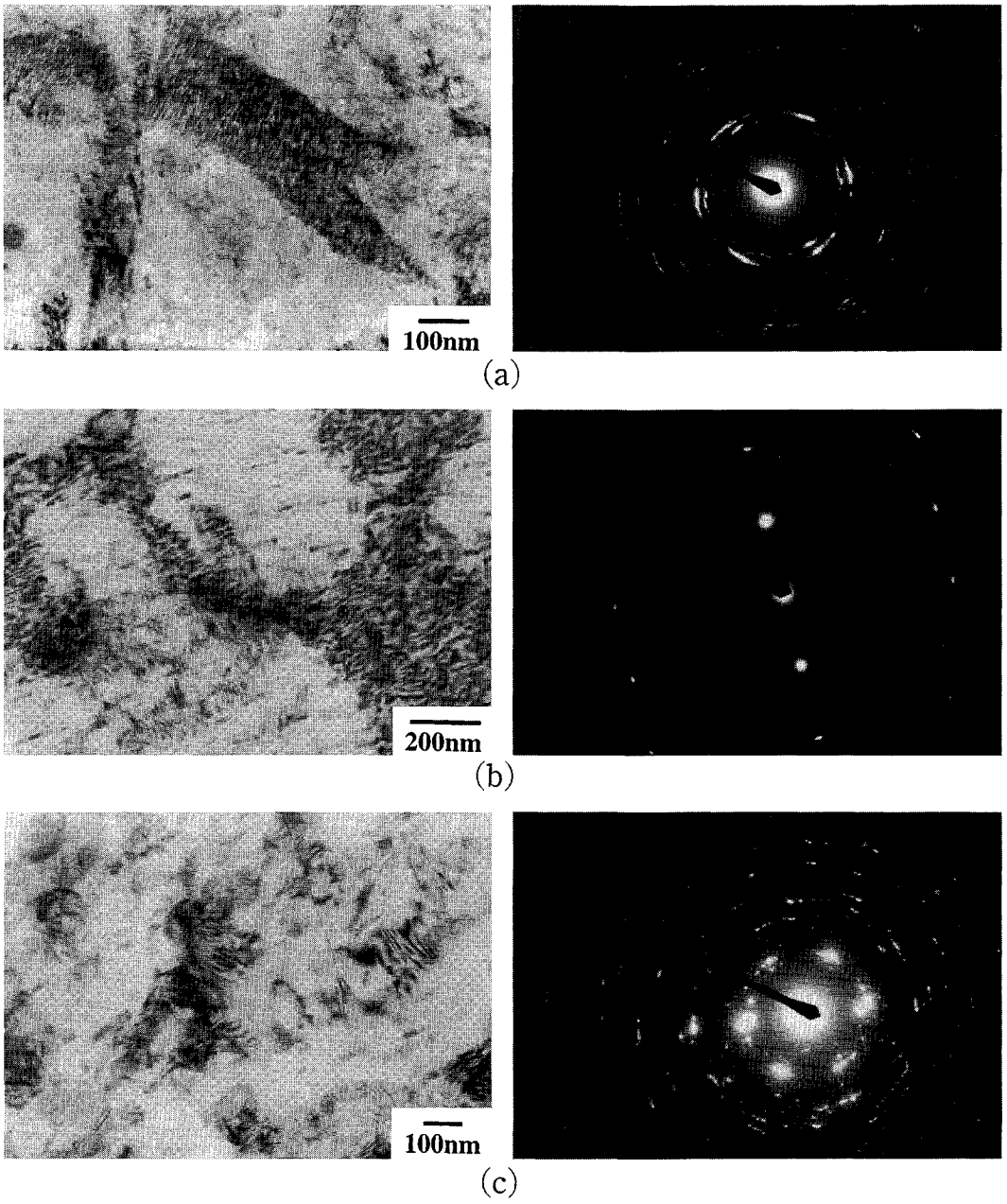

Fig. 7 TEM microstructures and diffraction patterns after straining $e = 0.5$. (a) state 1; (b), (c) state 2.

Table 2 Diffusivity of diffraction spots (Degr) toward azimuthal direction.

	$e = 0.5$	$e = 1$	$e = 4$	$e = 7$
State 1	---/6–15	5/12–18	7–15/9	10–18/---
State 2	4.5*/3.5	10–16/4–8	19–36/---	---/---

*The numerator gives values for areas of recrystallized grains; the denominator for areas of non-recrystallized structure.

second type.

In the state 1 further deformation leads to increasing volume fraction of crystallite structure which is similar to that described above for the state 2 after $e = 4$ (Fig. 10(a)). The special feature of the structure is a large volume of new grains of first and second type. The grains of third type have an elongated shape (100–300 × 50–80 nm) and usually are fully revealed in reflected position in spite of high dislocation density. Notably, no fully crystallite structure was evolved even after $e = 7$.

On the contrary the structure in the state 2 is fully granular one after $e = 7$. The grains of the first and second type are dominating in the structure (Fig. 10(b)). The volume fraction of crystallites of third type reduces. The image contrast in new grains indicates elastic stress fields even in case when the lattice dislocations are observed within these grains.

4. Discussion

Analysis of experimental results shows that granular structure is evolved during IPS in the ZK60 alloy at ambient temperature ($T = 0.31T_m$). This structure is strongly different from recrystallized structure formed at high deformation tem-

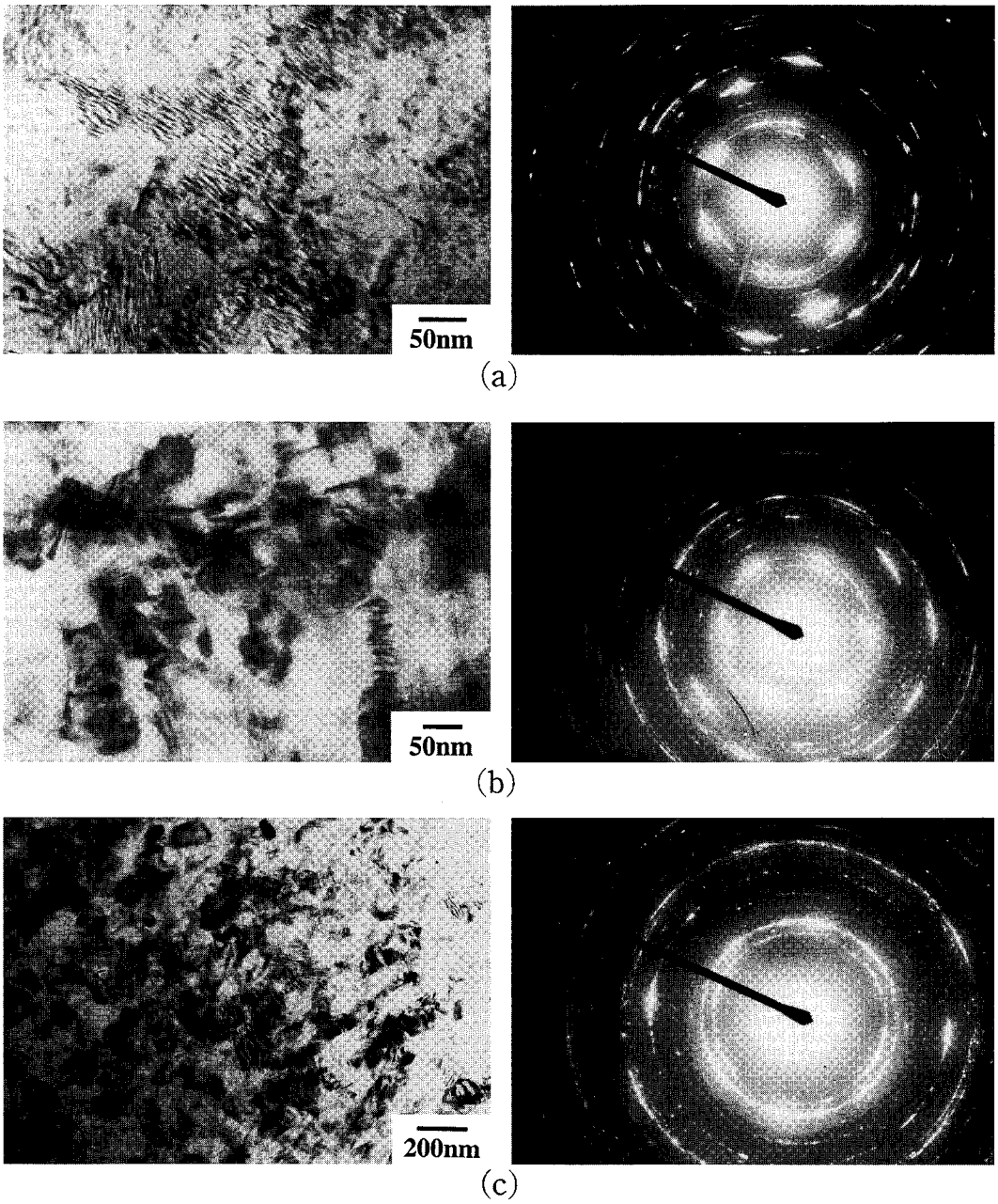

Fig. 8 TEM microstructures and diffraction patterns after straining $e = 1$. (a), (b) state 1; (c) state 2.

peratures.[10] It is apparent from data of X-ray analysis and TEM observation that boundaries of nanometer-scale grains evolved are the sources of long range stress fields. These stress fields originate from walls of grain boundary dislocations[7] and provide large elastic distortion of lattice inside the grains.[11] Unusual effect of phase composition of the magnesium alloy on the size of grains evolved and the rate of granular structure formation is caused by operation of a specific mechanism resulting grain refinement at room temperature. This type of microstructural evolution was named as low temperature dynamic recrystallization (LTDRX).

4.1 The mechanism of grain formation

The twinning occurs in the both states of ZK60 alloy with initiation of plastic deformation. However, the twinning does not lead to "twin" DRX as in pure magnesium[5] due to the fact that in the ZK60 alloy the dissociation of lattice dislocations trapped by boundaries does not occur at ambient temperature.[12] Respectively, the migration of twin boundaries is not developed. The twinning results in subdivision of initial grains into areas surrounded by twin boundaries. The twin boundaries play the role of barriers for dislocation glide due to accumulation of dislocations and provide an appearance of areas where single slip can occur.[13] It seems that twinning in the magnesium alloy with low value of stacking fault energy plays a similar role as low energy dislocation structure in fcc materials with high value of stacking fault energy.[13]

Dislocation slip in the both states of ZK60 alloy developing along basal planes prevails. However, the data of texture analysis shows that non-basal slip should operate after high strain. This conclusion is supported by observation of non-basal slip at low temperatures for magnesium.[14,15] The initiation of sec-

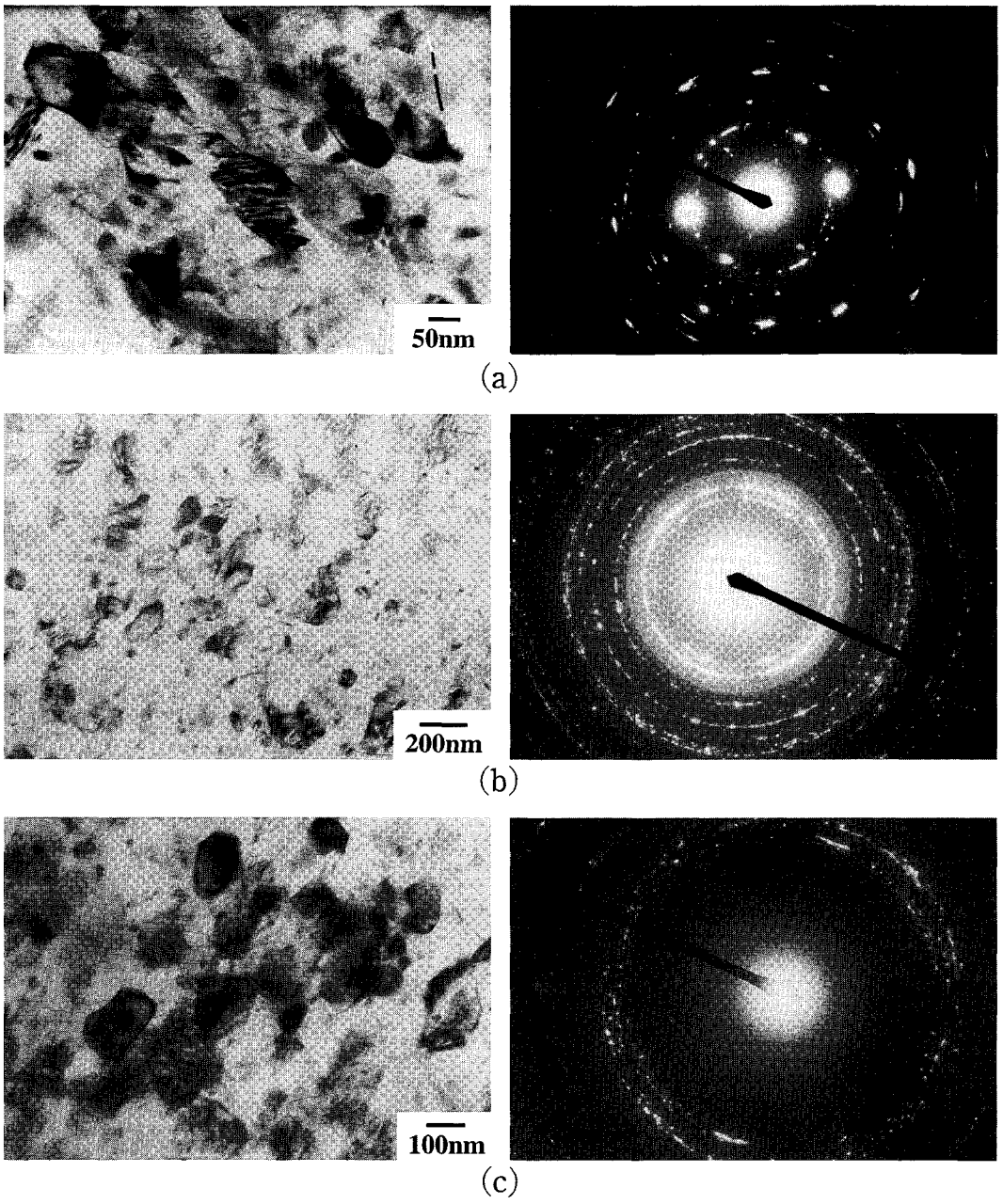

Fig. 9 TEM microstructures and diffraction patterns after straining $e = 4$. (a) state 1; (b), (c) state 2.

ondary slip in adjacent areas separated by twin boundaries can result in formation of high angle boundaries inside these areas. Details of this mechanism are still unknown. However, it is apparent from TEM observation that new grains form due to an extensive bend of crystal lattice. It yields ultra-high internal elastic strain. The mechanism of grain formation serves as a mechanism for relaxation of this internal stresses. The driving force of this process is a decrease of total system energy due to decreased high elastic stresses.

The schema for mechanism of nanometer-scale grain formation is presented in Fig. 11. Dislocation pile-ups are formed in parallel basal planes. It provides strong bending crystal lattice. Superposition of internal and external stress fields can reach a critical value for non-basal slip systems into areas of elastic imperfection. Thus, the possibility for non-basal slip appears in the ZK60 alloy at ambient temperature. Appearance of dislocations with non-basal Burgers vectors provides feasibility for the formation of areas of high-angle boundaries due to rearrangements of lattice dislocations. Mechanism of this rearrangement is under examination and is not clear till now. However, it is possible to conclude that the new grains are formed at the place of areas of great elastic imperfection. Dislocations rearrange from pile-ups (Fig. 11(a)) to dislocation boundaries with high angle misorientation (Fig. 11(b)). These boundaries contain the networks of grain boundary dislocations which can be represented equally as junction disclinations.[16] The further deformation of material with such granular structure results in gradual relaxation of internal elastic strain originated from these grain boundary dislocations of high density.

Plastic deformation to large strains leads to spreading of texture. Only one deformation mechanism may be responsi-

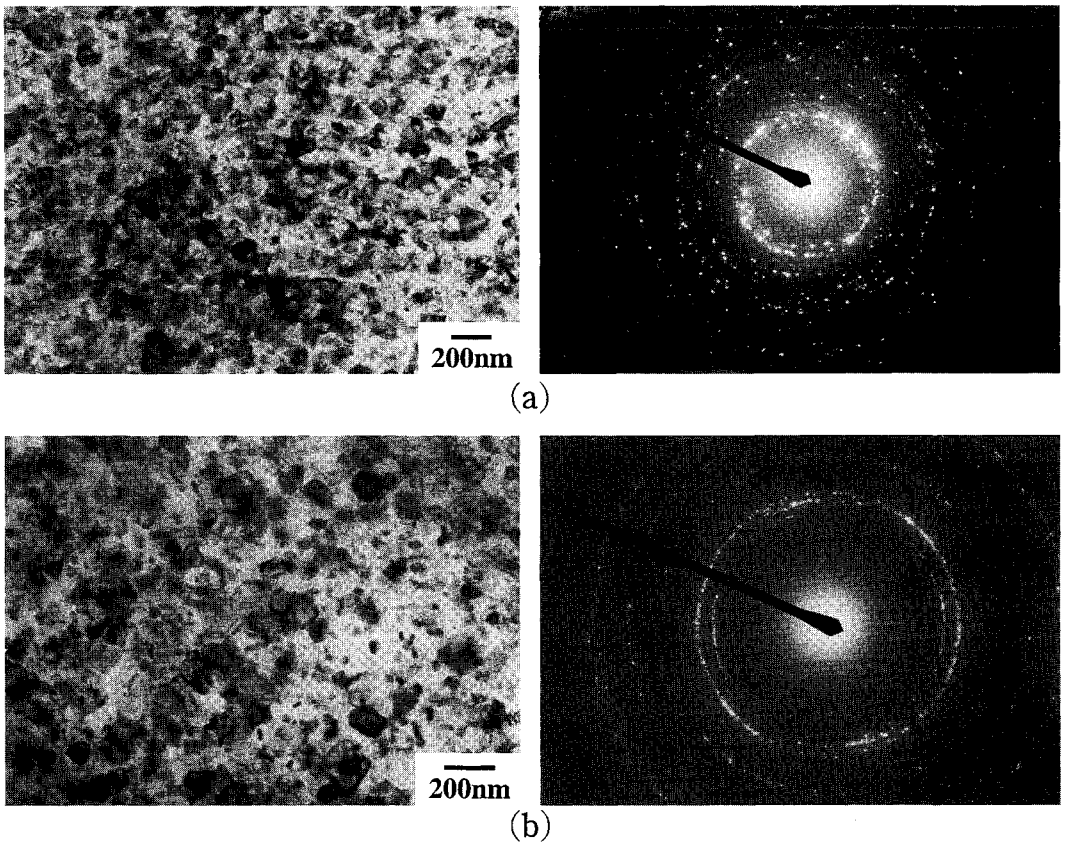

Fig. 10 TEM microstructures and diffraction patterns after straining $e = 7$. (a) state 1; (b) state 2.

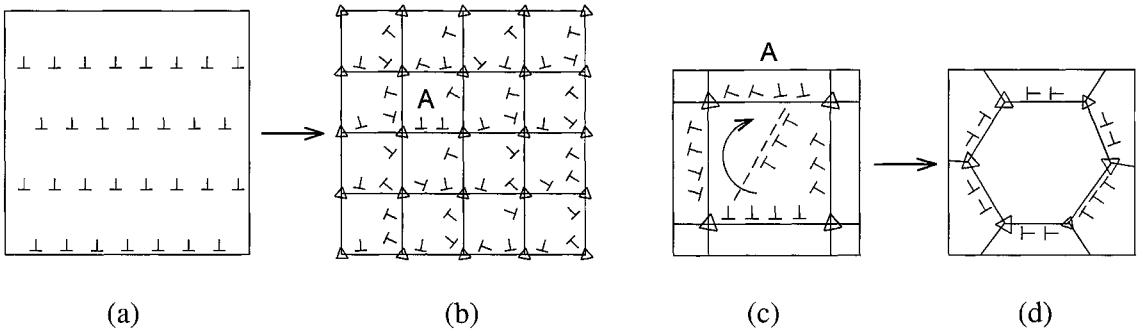

Fig. 11 Schematic illustration of microstructural evolution in the ZK60 magnesium alloy.

ble for this process. It is grain boundary sliding.[17] The contribution of grain boundary sliding into total deformation must exceed 50% in order to provide a texture spreading. The low value of coefficient of strain rate sensitivity, m, observed is not typical for high temperature grain boundary sliding.[12,17] Probably, the grain boundary sliding occurs in nanometer-scale grains by operation of a specific mechanism. It is well known that grain boundary sliding accelerates the spreading of grain boundary dislocations.[12,17] A decrease in density of grain boundary dislocations causes a reduction of the internal elastic strain. Concurrently, a transition from rectangular grain shape to essentially equiaxed shape takes place at a very large strain (Figs. 11(c) and (d)). Notably this process is not accompanied by a reduction in microhardness. Probably, it is caused by the fact that boundaries containing low density of grain boundary dislocations become impenetrable for gliding lattice dislocations. As a result, the Hall-Petch relationship becomes operative and an increment in yield stress caused by grain refinement is observed.

4.2 The influence of phase composition on low temperature DRX

Analysis of experimental results shows that phase composition affects the mechanisms of deformation and LTDRX. In the state 2 the twinning is less extensive and LTDRX initiates at a lower strain than in the state 1. The results obtained indicate that the dislocation slip in the state 2 is more homogeneous than that in the state 1. As a result, no dislocation features were observed at surface of samples of the state 2. The uniform slip is favorable for the formation of the large number of mutually misorientated dislocation pile-ups. The process of low temperature DRX is facilitated in this case.

New grains homogeneously appear in whole material volume. Besides aging leads to increased role of the non-basal slip as was shown by the texture analysis. Therefore, the favorable conditions are developed for the formation of dislocation boundaries in material volume. All these factors contribute to acceleration of LTDRX with an increase in volume fraction of secondary phases. On the other hand the second phase particles play a role of effective barrier for dislocation motion and new grains may nucleate heterogeneously on interphase boundaries. This phenomena is similar to particle stimulated nucleation during recrystallization at high temperatures.[18)]

In the state 1 the localization of plastic deformation causes larger internal elastic strains due to enhanced dislocation density in the slip bands. Probably, high internal stress fields hinder rearrangements of lattice dislocations. In addition, an interaction between stress fields originated from grain boundary dislocation networks and stress fields originated from strongly distorted lattice of supersaturated solid solution takes place. Both these factors contribute to increase a distortion of crystal lattice and may be a reason for difference of the contributions of the internal elastic strain and coherent domain size into the X-ray physical line broadening for the two states of the magnesium alloy (Figs. 6(c) and (d)).

4.3 The influence of chemical composition

Comparision with the results for pure magnesium[5)] shows that a very strong influence of a chemical composition on the size of recrystallized grains is caused by specific features of non-equilibrium boundaries. The presence of dislocation networks into grain boundaries leads to increasing role of the restraining force for low temperature DRX. The latter becomes the factor that controls a size of recrystallized grains. The role of the drag effect of solute atoms is minor. The solution-alloying affects the ability of non-equilibrium grain boundaries to recover and, therefore, influences a grain size. Grain boundaries of magnesium can absorb grain boundary dislocations[12)] and in some cases reach an equilibrium state at room temperature. This leads to decreased long-range internal stress fields and facilitates grain boundary migration. In the magnesium alloy the recovery process almost does not occur on grain boundaries. The interaction of grain boundary stress fields with internal stresses originated from solid solution creates the largest barriers on the way of grain boundary migration. It causes a great difference between the size of grains formed in magnesium and magnesium alloy during IPS at ambient temperature.

5. Conclusions

(1) Intense plastic straining of ZK60 magnesium alloy results in producing ultrafine grain structure.

(2) Prior annealing provides a significant increase in rate of nanometer-scale grain formation during torsion under high pressure. A fully grained structure was observed after a true strain of 4 in the aged state of the magnesium alloy. The formation of crystallite structure was not finished even after $e = 7$ in the quenched state of the magnesium alloy.

(3) The strong microhardness increment was found at true strain less than 1. Following deformation results in gradual increase in microhardness. In the aged state of the magnesium alloy a steady-state can be observed after a true strain of 4.

(4) The size of new grains formed was found to be smaller in the quenched state of the magnesium alloy than in the aged state.

(5) It was shown that the enhanced volume fraction of secondary phase particles provided a very high uniformity of dislocation slip. It facilitates the process of low temperature dynamic recrystallization.

Acknowledgement

One of the authors (A.G.) wishes to express his gratitude to the Alexander von Humboldt Foundation for the award of a research fellowship.

REFERENCES

1) A. N. Belyakov and R. O. Kaibyshev: Nanostruct. Mater. **6** (1995) 893–896.
2) Y. Iwahashi, Z. Horita, M. Nemoto and T. G. Langdon: Acta Mater. **46** (1998) 3317–3331.
3) R. Z. Valiev, Yu. V. Ivanesenko, E. F. Rauch and B. Baudelet: Acta Mater. **44** (1996) 4705–4712.
4) S. L. Semiatin, V. M. Segal, R. E. Goforth, N. D. Frey and D. P. DeLo: Metall. Trans. **30A** (1999) 1425–1435.
5) R. Kaibyshev and O. Sitdikov: Z. Metallkd. **85** (1994) 738–743.
6) R. Z. Abdulov, R. Z. Valiev and N. A. Krasilnikov: J. Mater. Sci. Lett. **9** (1990) 1445–1447.
7) M. Mabuchi, K. Ameyama, H. Iwasaki and K. Higashi: Acta Mater. **47** (1999) 2047–2057.
8) N. A. Smirnova, V. I. Levit, V. I. Pilyugin, R. I. Kuznetsov, L. S. Davydova and V. A. Sazonov: Fiz. Met. Metalloved. **61** (1986) 1170–1177.
9) V. Y. Gertsman, R. Birringer, R. Z. Valiev and H. Gleiter: Scripta Metall. Mater. **30** (1994) 229–234.
10) R. Kaibyshev and A. Galiev: *Proc. 3rd Int. Conf. on Recrystallization and Related Phenomena*, ed. by T. R. McNelly, (Monterey Institute of Advanced Studies, 1997) pp. 239–246.
11) A. Belyakov, T. Sakai, H. Miura and R. Kaibyshev: Philos. Mag. Lett. **80** (2000) 711–718.
12) O. A. Kaibyshev and R. Z. Valiev: *Grain Boundaries and Properties of Metals*, (Metalurgia, Moscow, 1987) pp. 213.
13) B. Bay, N. Hansen, D. A. Hughes and D. Kuhlmann-Wilsdorf: Acta Metall. Mater. **40** (1992) 205–219.
14) T. Obara, H. Yoshinaga and S. Morozumi: Acta Metall. **21** (1973) 845–853.
15) J. F. Stohr and J. P. Poirier: Philos. Mag. **25** (1972) 1313–1329.
16) V. V. Rubin, A. A. Zisman and N. Yu. Zolotorevsky: Acta Metall. Mater. **41** (1993) 2211–2217.
17) O. A. Kaibyshev: *Superplasticity of Alloys, Intermetallides and Ceramics*, (Springer-Verlag, Berlin, 1992) pp. 317.
18) F. J. Humphreys: Acta Mater. **25** (1977) 1323–1344.